Iran J Public Health, Vol. 54, No.9, Sep 2025, pp.1938-1953

Original Article

Optimizing a Subunit Vaccine of *Mycobacterium tuberculosis* Using In-Silico and In-Vitro Approaches

Zaiqin Ling [1], ****Muhammad Ahsan Naeem*** [2,3]

1. *Department of Tuberculosis, Shandong Public Health Clinical Center, Shandong University, Jinan, 250013, China*
2. *College of Veterinary Medicine, Huazhong Agricultural University, Wuhan 430070, China*
3. *Department of Basic Sciences (Pharmacology), University of Veterinary and Animal Sciences, Lahore, Pakistan (Narowal Campus- 51600)*

***Corresponding Author:** Email: muhammadahsannaeem@ymail.com

(Received 18 Jan 2025; accepted 25 Apr 2025)

Abstract

Background: The present study addresses the development of a novel subunit vaccine (SV) to combat tuberculosis (TB).

Methods: The research used immunoinformatics to develop a subunit vaccine with 7 MHC-I, 3 MHC-II, and 7 B-cell epitopes joined by AAV, GPGPG, and KK linkers. It involved Mtb protein Rv0577 and PADRE sequence as an adjuvant. TLR2 binding affinity (Kd, nM) was determined through PRODIGY. In-silico evaluations determined allergenicity, antigenicity, and physicochemical properties. The vaccine was presented in an AAVDj/8 system, intracellular expression was verified, and the copy number was identified using qPCR and qRT-PCR.

Results: The web tools confirmed the stability, non-allergenicity, and high immunogenicity of the vaccine (0.5673 < 0.4). PRODIGY tool depicted good SV-TLR2 binding (ΔG = -8.8 kcal/mol, Kd = 330 nM) with 59 intermolecular contacts, indicating possible TLR2 activation. Indirect immunofluorescence showed the expression of intracellular proteins. Viral titers, determined by 10-fold serial dilution up to 10^3, showed a detectable titer, and copy numbers (10^9/mL–10^{11}/mL) proved productive viral replication and significant vaccine effectiveness.

Conclusion: This comprehensive methodology, from epitope selection to in-vitro testing, establishes a robust foundation for further exploring and advancing this SV.

Keywords: Tuberculosis; Bacillus Calmette-Guérin (BCG) vaccine; Immunoinformatics; Subunit vaccine; Adeno-associated virus (AAV) vector

Introduction

Tuberculosis (TB) is still one of the 21st century's top 10 killer diseases, as classified by the WHO (1). Mycobacterium tuberculosis (Mtb) induces pulmonary and extra-pulmonary TB via organ lesions (2). The emergence of drug-resistant TB highlights the importance of new vaccine approaches (3). Immunoinformatics-guided subunit vaccines (SVs) hold potential by focusing on immunogenic epitopes (4), capitalizing on knowledge of Mtb's secretory pathways for ra-

Copyright © 2025 Ling et al. Published by Tehran University of Medical Sciences.
This work is licensed under a Creative Commons Attribution-NonCommercial 4.0 International license.
(https://creativecommons.org/licenses/by-nc/4.0/). Non-commercial uses of the work are permitted, provided the original work is properly cited
DOI: https://doi.org/10.18502/ijph.v54i9.19861

tional vaccine design (5). Although BCG is protective, its inconsistent efficacy, particularly against adult pulmonary TB, requires other strategies (6, 7). Mtb has three primary secretory pathways: the general secretory (Sec) pathway, twin-arginine translocation (TAT) pathway, and Type VII secretory pathway (T7SS/Esx) (9). These pathways secrete virulence factors and enable immune evasion (10). SecA2 of the Sec pathway secretes evasive effectors, whereas the TAT pathway secretes folded proteins (11). The Esx pathway secretes extremely antigenic proteins such as ESAT-6 and CFP-10, which help in virulence (12).

Though there has been progress in the understanding of these pathways, current SVs target restricted antigens and do not fully involve secretion mechanisms (8). Although certain significant contributions to knowledge about *Mtb* secretory systems, and more significantly the Sec, TAT, and Type VII, have been established, the void at the core is around efficient SV that would integrate these systems best (13). An effective SV should support multiple secretory pathways to maximize immunogenicity. Peptide vaccines ensure specificity, safety, and long-term immune responses (14). Antigenic targets are SecA2 (Sec system), Rv2525c (TAT system), and Esx-1 to Esx-5 (Esx system) (12, 15, 16).

We aimed to develop an immunoinformatics-guided SV for TB, analyzing its in-silico properties as well as its in-vitro characterization, with the aim of creating an effective vaccine against TB.

Materials and Methods

Collection of protein sequences for vaccine design

Protein sequences of 23 Esx, 10 Sec system, and 5 TAT system proteins of *Mtb* were retrieved from Mycobrowser http://www.mycobrowser.epfl.ch/ in FASTA format. Rv0577, TLR2 agonist protein (TB27.3, PDB ID: 3OXH), the amino acid sequence was recovered from the Mycobrowser database to be used as an adjuvant for the SV.

MHC-I/-II binding and B cell epitopes prediction

MHC-I binding epitopes (9-mer length) of *Mtb* were predicted using an online 'immune epitope database (IEDB)' analysis resource (http://tools.immuneepitope.org/mhci/) (17). Linear B-cell epitopes were predicted using the ABCPREDS server (http://crdd.osdd.net/raghava/abcpred/ABC_submission.html) for the vaccine construct. Epitopes were selected by keeping a threshold > 0.9 and a length of 20 amino acids (18).

Multi-epitope subunit vaccine construct

The last vaccine construct combined 7 MHC-I, 3 MHC-II, and 7 B-cell epitopes with AAY, GPGPG, and KK linkers for immune presentation and epitope integrity (19-22). EAAAK preserved domains, GPGPG and GPSL induced immunity (23), GGGS provided flexibility, and KK facilitated antigen processing (24). AAY stabilized protein (25). Rv0577 (PDB: 2Z7X) acted as an adjuvant (26), with a PADRE sequence that increased the immune response (27, 28) (Fig. 1).

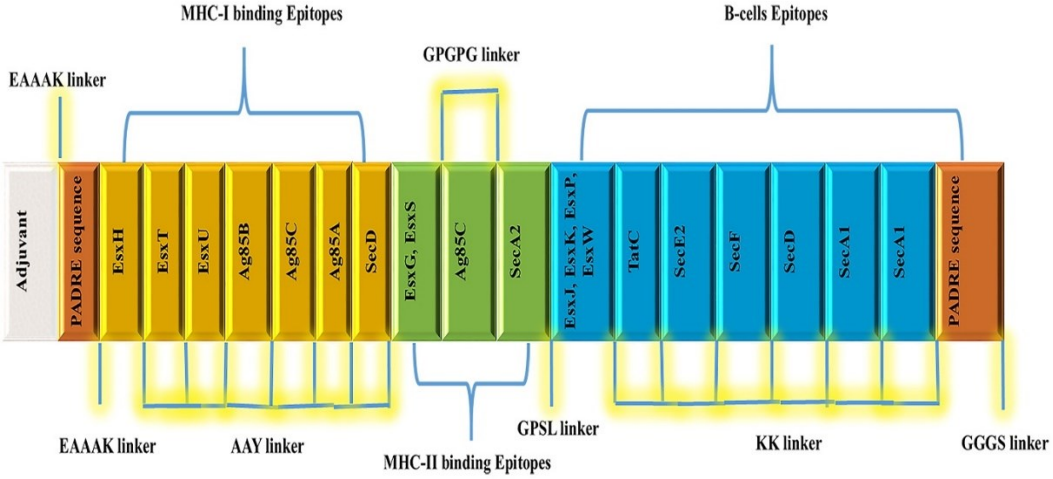

Fig. 1: Schematic diagram of final subunit vaccine construct

The 576-amino-acid multi-epitope vaccine consists of a 261-residue adjuvant, MHC-I (284–346), MHC-II (347–405), and B cell epitopes (406–559). PADRE was incorporated at 262–284 and 560–576. Linkers: EAAAK (adjuvant-MHC-I), AAY (MHC-I–MHC-II), GPGPG (MHC-II–B cell), and KK (B cell epitopes).

Prediction of physciochemical parameters, allergenicity, antigenicity analysis

For physico-chemical parameters determination, the ProtParam web server (29), a part of the Expert Protein Analysis System (EXPASY), was used. Allergenicity prediction was done by employing the AlgPred web tool (http://www.imtech.res.in/raghava/algpred/) (30). ANTIGENpro (http://scratch.proteomics.ics.uci.edu/) was applied for the prediction of the antigenicity of the vaccine protein.

Docking of SV with mouse TLR2 receptor

To dock SV into the mouse TLR2 receptor, plots of secondary and tertiary structures were needed. PSIPRED server (http://bioinf.cs.ucl.ac.uk/psipred/) was applied to predict the secondary structure, and RaptorX (http://raptorx.uchicago.edu/) was applied to model the 3D structure. 3D modeling was visualized using Discovery Studio (Disco 2.1). TLR2 (PDB ID: 2Z7X) of RCSB was docked with SV using PatchDock (http://bioinfo3d.cs.tau.ac.il/PatchDock/) (31, 32).

Reverse translation, codon optimization, and in silico cloning

The vaccine protein was reverse-translated to a nucleotide sequence with SMS2 (http://www.bioinformatics.org/sms2/rev_trans.html) and codon-optimized through JCAT (http://www.jcat.de) for *Mus musculus*. The optimized sequence was cloned into pAAV through SnapGene, inserting it with XhoI digestion (33).

In-vitro cloning

The codon-optimized nucleotide sequence of the vaccine construct was sent to the Genecreate® Company for synthesis by removing the Rv0577 (TLR2 agonist) sequence and inserting the Flag tag at the N- terminal of the remaining nucleotide sequence. Rv0577 was removed because the AAV-Dj virus penetrates the cells and binds to the intracellular receptor TLR9 (34, 35, 36) rather than the cell surface receptor, TLR2. After receiving the desired synthesized sequence from the company, the sequence was amplified by designing primers (sequence given in Table 1) and then cloned (homologous recombination) in pAAV-CMV-eGFP vector by digesting it at the *Xho*I restriction site.

Table 1: Primer sequences

Plasmid	Primer Name	Forward Primer sequence 5`-3`	Reverse Primer sequence 5`-3`	Remarks
pAAV-CMV-eGFP	Temp-1	gaggctgctgccaaggctaagttg	cttgagggtccaagcagccacgaac	All three are used consecutively for SV amplification and insertion of pAAV-CMV-eGFP plasmid.
	Temp-2	atggattacaaagacgatgacgataaggaggctg	gctgccgccgccggcggcggccttgagggtccaa	
	Temp-3	ccgatccagcctcccatggattaca	caccatacgcgtgacgctgccgccg	
	ITR	ggaacccctagtgatggagtt	cggcctcagtgagcga	DNA and RNA copy number detection in AAV-eGFP and AAV-SVeGFP viruses
	eGFP	acagggaattccaccatggtgagcaag	ttgaagaagatggtgcgctcc	eGFP gene amplification

Intracellular SV expression

HEK293T cells (1×10^5 cells/well) were plated in a 24-well plate and grew in DMEM (10% FBS, 1% penicillin-streptomycin) and incubated (37°C, 5% CO_2) for 24 h. Transfection of pAAV-CMV-eGFP or pAAV-CMV-SVeGFP (1 µg) was achieved with Lipofectamine 2000 or PEI in Opti-MEM. Cells were fixed (4% paraformaldehyde), permeabilized (0.1% Triton X-100), blocked (5% BSA), and stained with Flag-tag antibody and Alexa Fluor 555 after 36 h. Red (vaccine protein-eGFP) and green (eGFP) were observed using fluorescence microscopy, verifying transfection and localization.

AAV virus generation

HEK293T cells were seeded on twenty 15 cm plates (Corning®), ten experimental virus packaging, and ten control virus packaging. Cells became 90% confluent one day before transfection. Cells were transfected with pepper vectors, pAAV-DJ/8, and pAAV in a 1:1:1 ratio by Lipofectamine™ (Invitrogen®). Cells were left at room temperature for 20 min after 48-72 hours, agitated after 5 min, and left at 37 °C with 5% CO_2. 2% DMEM was changed after 24 hours and incubated for 48 hours. The presence of floating cells was a sign of viral production. Cells were centrifuged (1000 rpm, 5 minutes), washed, and frozen-thawed four times. Cleaned debris out (10,000 g, 10 minutes) and harvested AAV crude lysate. Frozen supernatant at -80°C in aliquots. Green fluorescence was seen in the control and experiment cells.

DNA and RNA copy number determination

For the determination of AAV copy number, qPCR was employed for convenience and expediency. A virus DNA (for DNA copy number) or cDNA template was made by combining 2 µL virus sample with 196 µL DMEM or ddH2O and adding 2 µL DNaseI, incubating at 37 °C for 1 hour, and then inactivating DNaseI by boiling (not needed for RNA copy number). pAAV-CMV-SVeGFP plasmid standards were made with a mass of plasmid 1.096×10^{-21} g and 1×10^{11} copies. Ten-fold serial dilutions were performed. qPCR was conducted with ITR primers, and Ct values were used in a linear equation ($y = ax + b$) to calculate viral copy numbers. For cDNA analysis, RNA was isolated with RNAiso Plus, reverse-transcribed with the ReverTra Ace qPCR RT Master Mix kit, and quantified by qPCR with SYBR Green Mix.

Results

Construction of multi-epitope vaccine sequence

The short-listed MHC-I/-II binding and B cell epitopes for TAT, Esx, and Sec systems are presented in Table 2-4, respectively.

Table 2: Selected MHC-I binding epitopes for mice

Protein Name	Peptide seq	Start	End	Allele	Percentile Rank	Method
Ag85B	WGPSSDPAW	220	228	H-2-Dd	0.1	Consensus (ann/smm)
Ag85C	GGPHAVYLL	57	65	H-2-Dd	0.1	-do-
Ag85A	WGPKEDPAW	223	231	H-2-Dd	0.1	-do-
EsxH,	IMYNYPAML	4	12	H-2-Kb	0.06	Consensus (ann/smm)
EsxT	ASALNEILI	66	74	H-2-Db	0.3	-do-
EsxU	STRLYHVL	66	73	H-2-Kb	0.26	-do-
SecD	VYLASKSSL	537	545	H-2-Kd	0.1	Consensus
						(ann/smm)

(Percentile rank threshold ≤ 0.3)

Table 3: Selected MHC-II binding epitopes for mice

Protein name	Peptide seq	Start	End	Allele	Percentile Rank	Method
EsxG, EsxS	QAEQAAMSAQAFHQG	31	45	H2I-Ad	0.05	Consensus (Smm/nn)
Ag85C	IPVAFLAGGPHAVYL	50	64	H2I-Ab	0.07	Consensus (Smm/nn)
SecA2	EFHRMAVDAFASLAA	736	750	H2-IAd	0.01	Consensus (Smm/nn)

(Percentile rank threshold ≤ 0.3)

Table 4: Selected B cell epitopes for mice

Protein Name	Epitope seq	Score	Start
TAT System			
TATC	PRNRRSRVNPDATMSLVDHL	0.92	12
Esx system			
EsxJ, EsxK, EsxP, EsxW	LVRDANNYEQQEQASQQILS	0.94	78
Sec system			
SecE2	DIRVARVIEQDMAVDSAGKI	0.92	34
SecF	TLTSDQTAKLRDALFEAFGP	0.92	143
SecD	YRVLGLLTALSLVASGSMVF	0.92	405
SecA1	EPAELAEFAAAAAAAAQQRS	0.92	848
	GGVTVATNMAGRGTDIVLGG	0.92	479

(Threshold score >0.90)

Physiochemical properties, Allergenicity, and antigenicity analysis

Physicochemical analysis yielded a molecular weight of 60.2 kDa (576 amino acids) and a theoretical pI of 6.34, showing neutrality at physiological pH. The protein contains 53 negative (Asp, Glu) and 50 positive (Arg, Lys) residues, with a formula of C2701H4186N730O793S19. It is stable (instability index: 33.88), hydrophobic (aliphatic index: 78.14), and hydrophilic (GRAVY: -0.061). It is non-allergenic (-0.59) and antigenic (0.5763). ANTIGENpro predicted three domains (1–336, 337–476, 477–576), with no disulfide bonds.

Molecular docking

The secondary structure of SV protein consists of 30.21% alpha-helices for stability, 27.95% beta-strands for strength, and 41.84% coils for flexibility (Fig. 2). RaptorX-predicted tertiary structure (Fig. 3A) and verified by ProSA (Fig. 3B) and Ramachandran plot (Fig. 3C) showed 409 residues (86.7%) in favorable regions. The high-quality model (90%) has 472 residues with 59 glycine and 42 proline. Mouse TLR2 docking is represented in Fig. 4 (37).

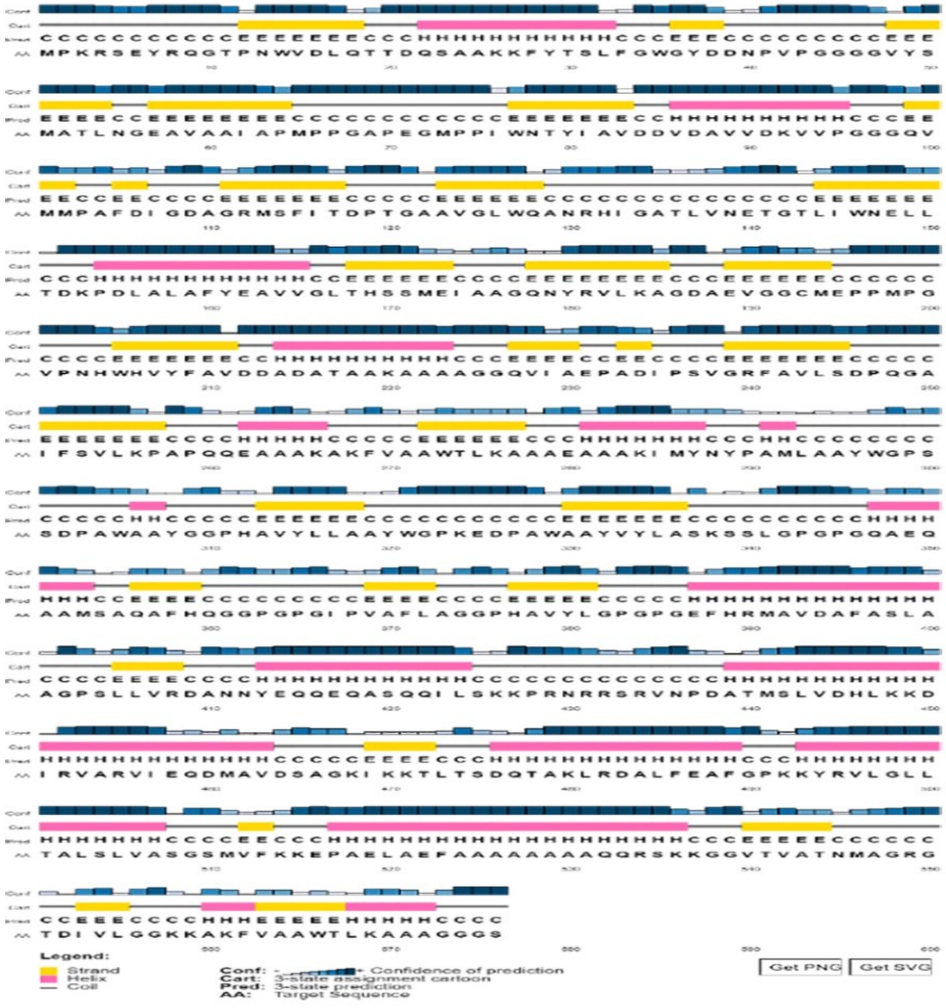

Fig. 2: Graphical illustration of secondary structure acquired for the SV construct elaborating beta-strands (27.95%), alpha-helix (30.21%), and coils (41.84%)

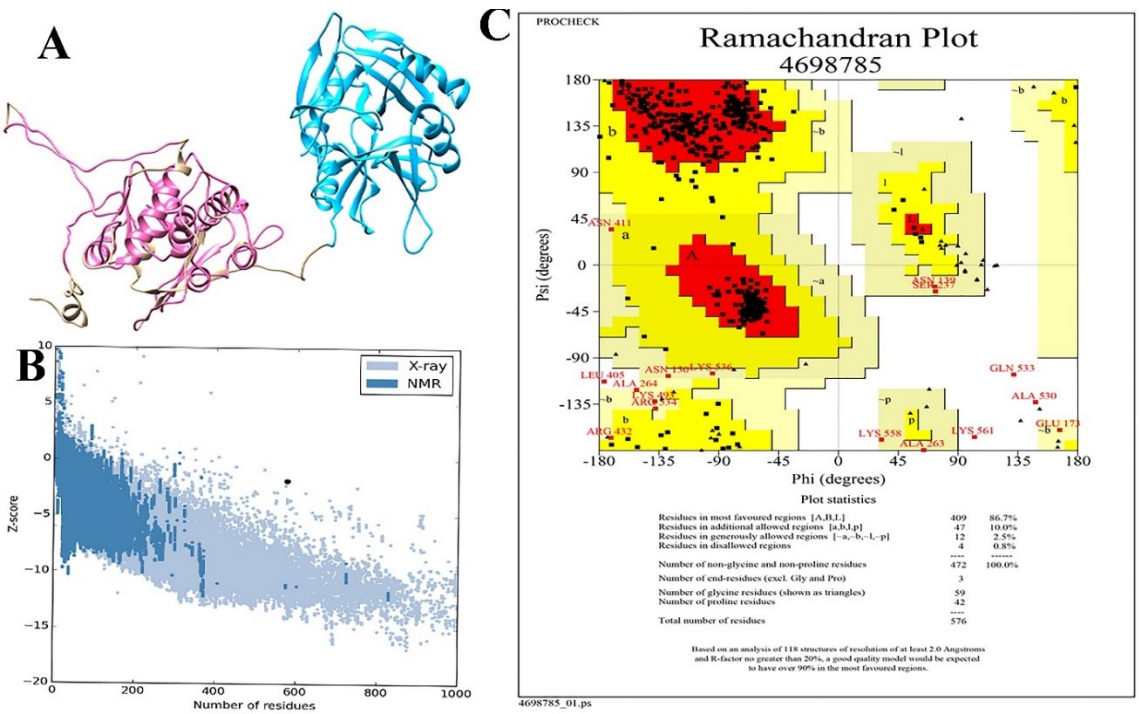

Fig. 3: Final SV model structure and validation. (A) Refinement of 3D multi-epitope vaccine model. (B) PROSA validation (Z-score: -1.52). (C) Ramachandran plot: 86.7% favored, 10% additional allowed, 2.5% generously allowed, and 0.8% disallowed

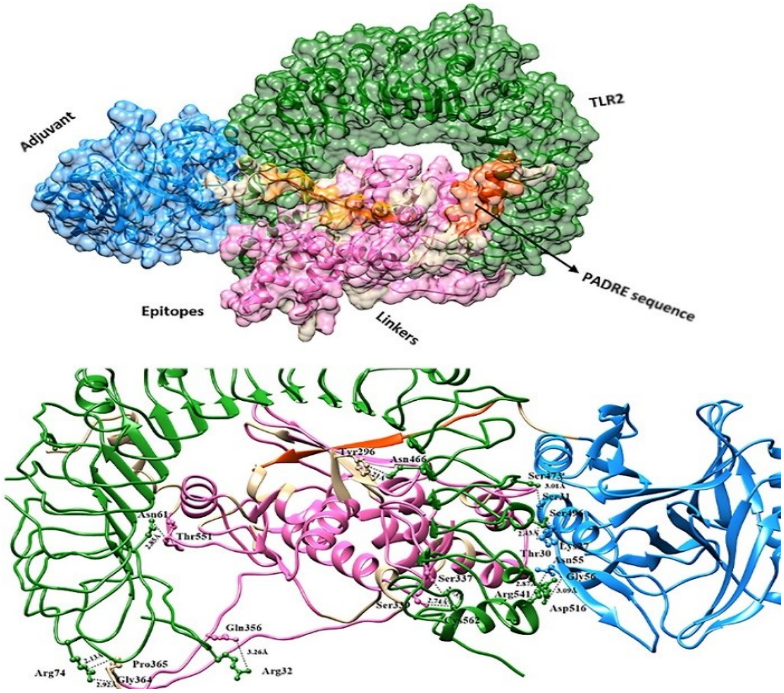

Fig. 4: A docked complex of TLR2 (PDB ID: 5D3I) with SV construct. (A & B) Receptor (TLR2) has been shown in green color, whereas cyan color represents the adjuvant and vaccine as a ligand (pink) in the docked complex obtained from the PatchDock server

Reverse translation, codon optimization, and in silico cloning

The SV protein sequence was reverse-translated to the nucleotide sequence. The total length of the reverse translated sequence was 1731 bp, and the codon-optimized sequence for expression in mice was shown in (The supplementary file). The codon adapted index (CAI) value was 0.72, and the GC content of *Mus musculus* was 41.8%. A graphical representation of the optimized sequence is shown in Fig. 5.

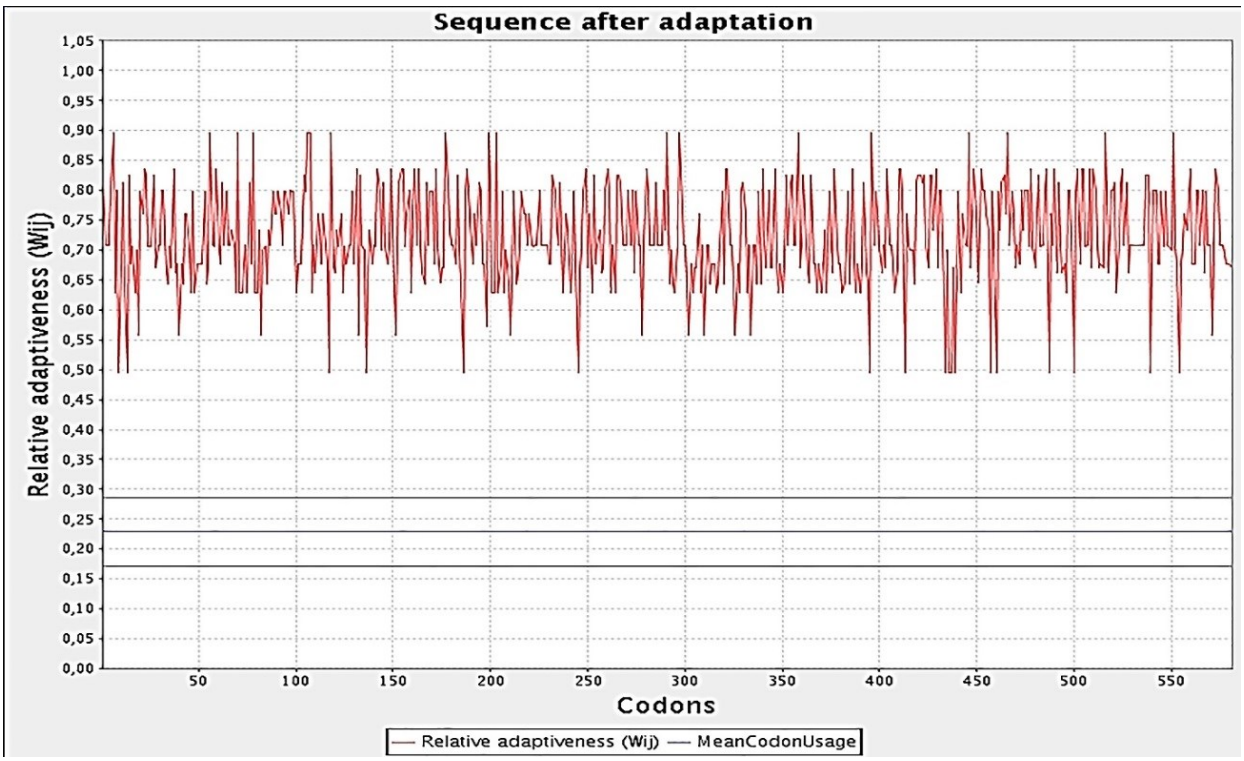

Fig. 5: Graphical presentation of codon-optimized sequence. Red peaks indicate the relative adaptiveness of each codon

The adapted sequence of vaccine protein was cloned in a mammalian expression vector pAAV-CMV-eGFP using the SnapGene tool to ensure the vaccine expression (Fig. 6 A & B).

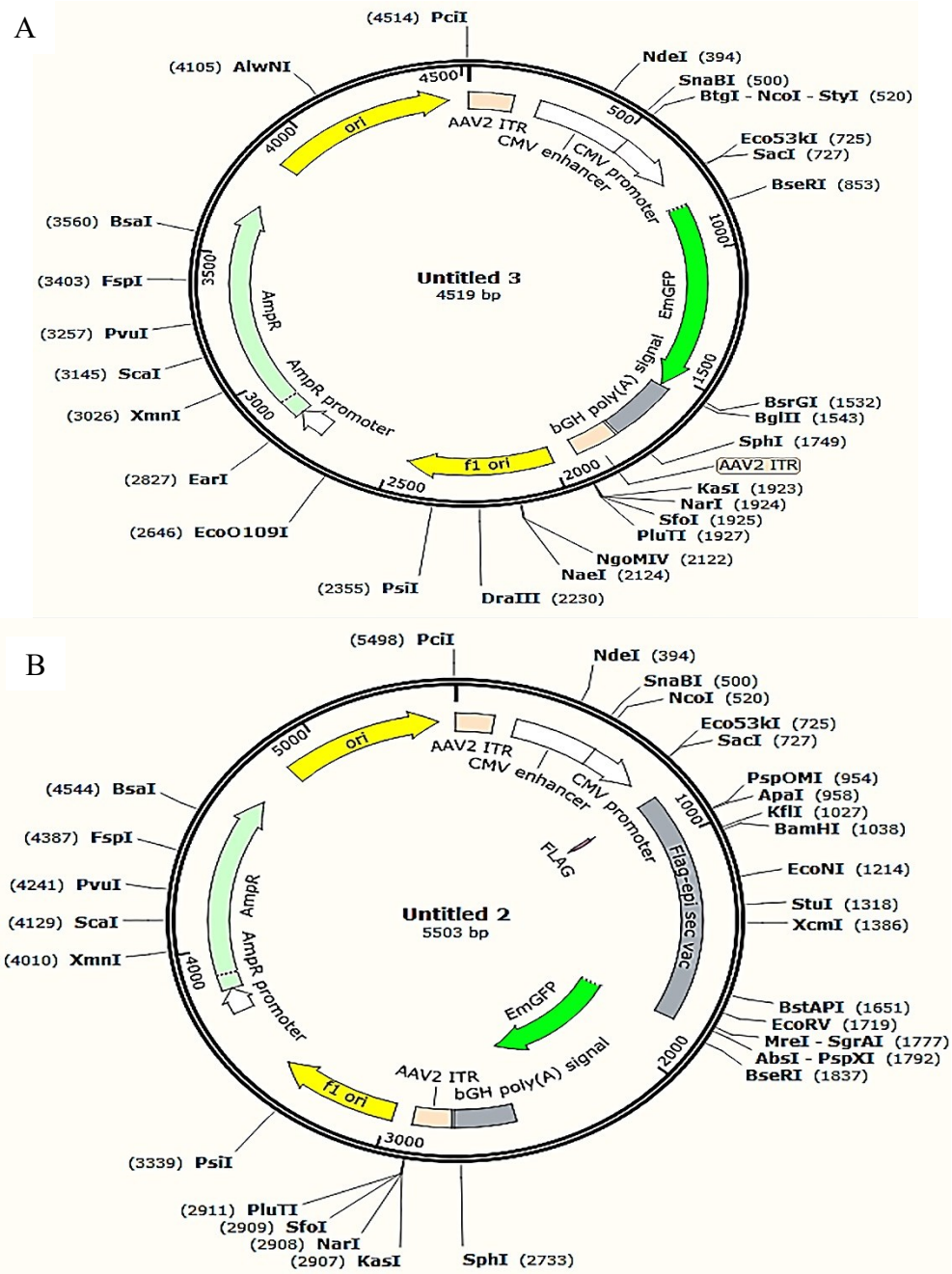

Fig. 6: A&B; Plasmid map showing control vector (pAAV-CMV-eGFP) and pAAV-CMV-SVeGFP

Removal of adjuvant and docking of vaccine protein with mouse TLR9

The tertiary structure of the N-terminal Flag-tagged amino acid sequence of SV was designed by applying RaptorX (Fig. 7A). SV fused with eGFP (SVeGFP) docked with mouse TLR9 receptor (PDB ID: 3WPG) is shown in Fig. 7B.

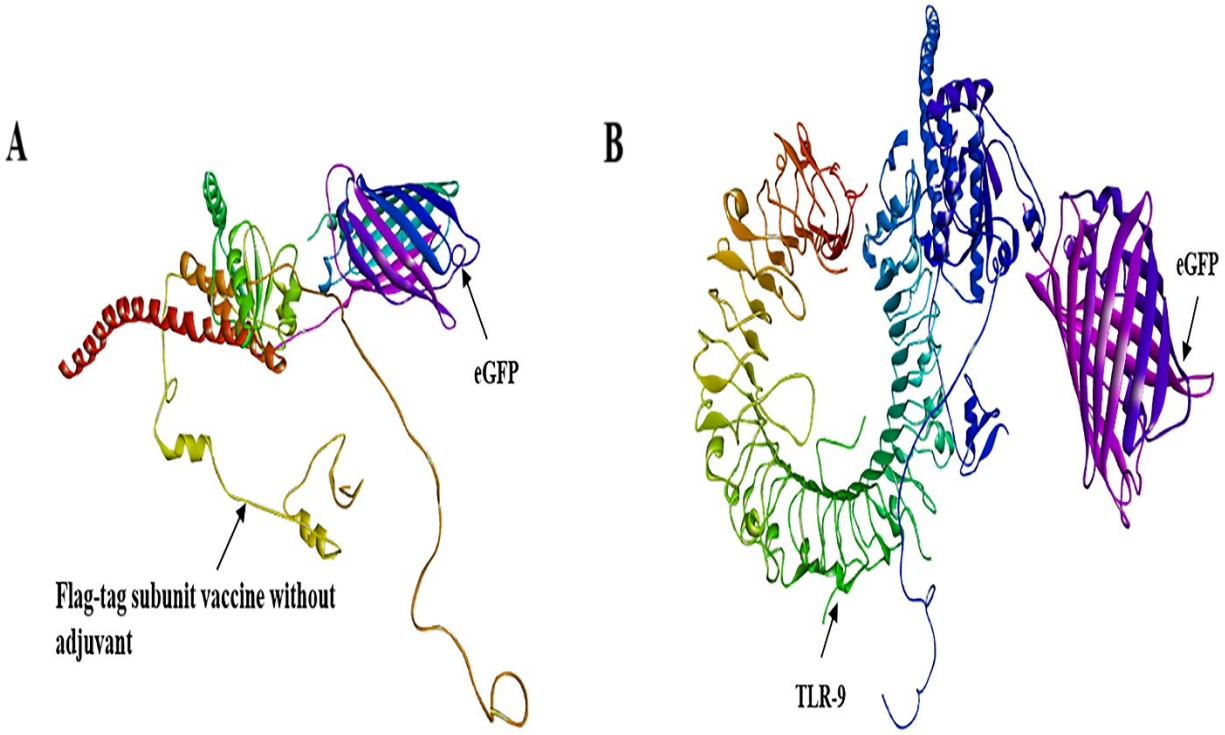

Fig. 7: A) SV structure without adjuvant and with N-terminal flag-tag. B) SV structure without adjuvant, with N-terminal flag-tag and C-terminal fused eGFP was docked with mouse TLR9 receptor (PDB: ID= 3WPG)

Cloning confirmation

Snapgene tool employed nucleotide sequences cloned into pAAV-CMV-eGFP vectors are shown in Fig. 6B. Primer sequences are given in Table 2. The product of 988 bp was run on 1% agarose gel for further work (Fig. 8).

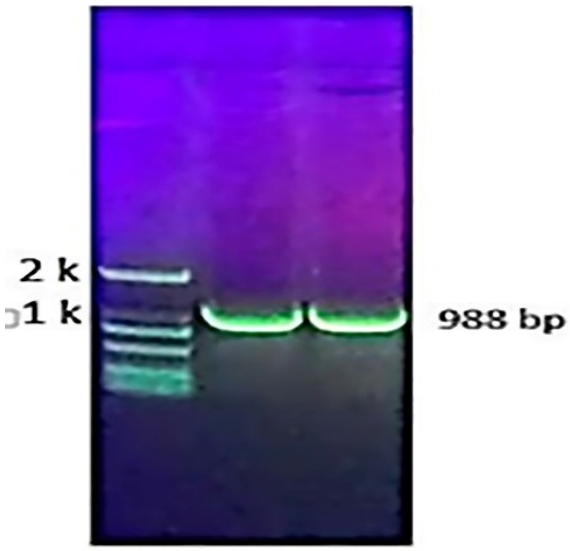

Fig. 8: Amplified subunit vaccine product

Successful cloning was confirmed by colony PCR and digesting the pAAVCMV-SVeGFP plasmid at the right (*Bgl*II restriction site) and left ITR regions (*Nde*I restriction site). Products were run on 1% agarose gel (Fig. 9).

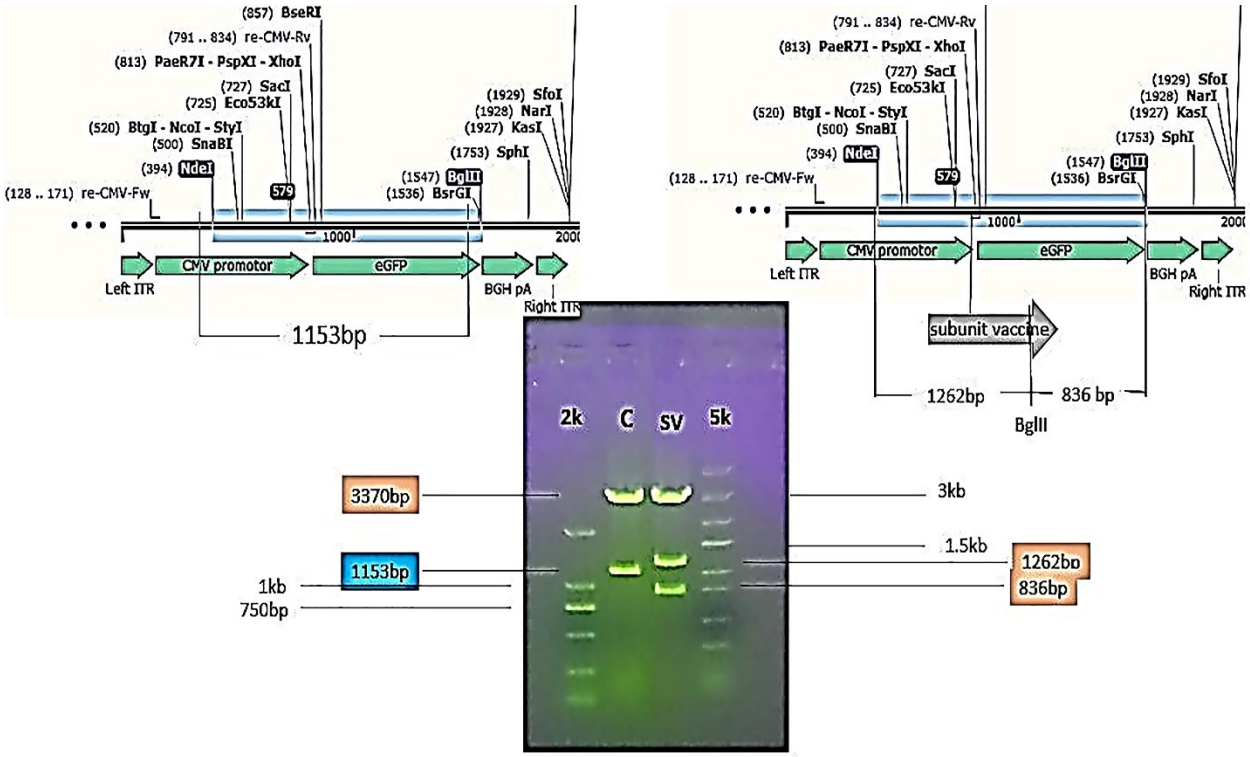

Fig. 9: Digestion of pAAV-CMV-SVeGFP plasmid to confirm the success of cloning both 2k (left) and 5k (right) markers were run on both sides of control plasmid (C) pAAV-CMV-eGFP and pAAV-CMV-SVeGFP plasmid

Subunit vaccine protein expression

Indirect Immunofluorescence Assay (IIFA) guaranteed the expression of the vaccine protein successfully as an eGFP fusion in HEK293T cells. Mouse monoclonal Flag tag antibody recognized the vaccine protein (SV), visualized by Alexa Fluor 555 goat anti-mouse secondary antibody. The red fluorescence prevailed in wells that were pAAV-CMV-SVeGFP-transfected, while control wells did not fluoresce, hence showing specificity. Red-green co-localization and co-expression in the majority of cells indicated successful fusion and localization. Approximately 75% of the cells were positive for eGFP and Flag fluorescence, confirming successful transfection and expression. The findings illustrate the potential of such constructs in the manufacture of vaccines and proteins (Fig. 10).

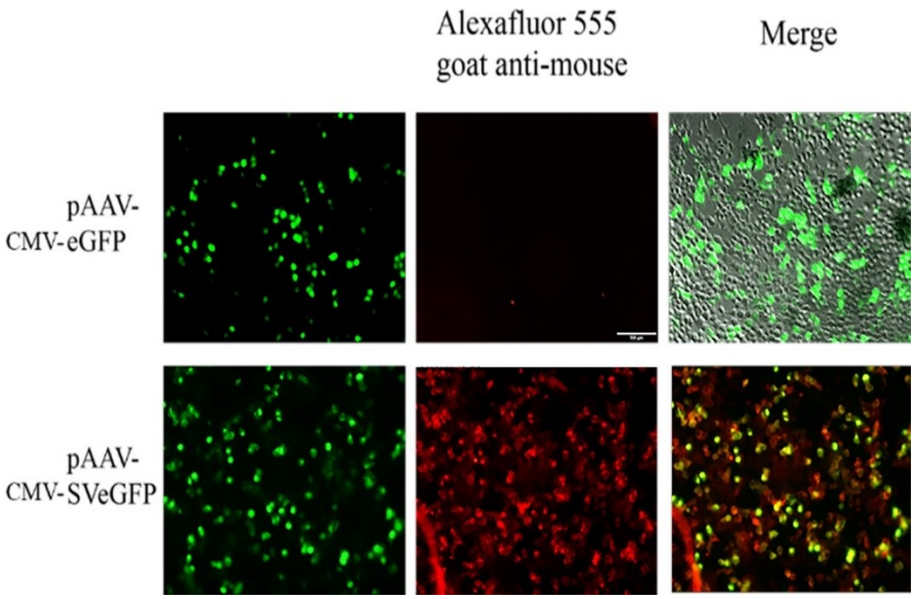

Fig. 10: Indirect Immunofluorescent Assay (IFA**)** to confirm the expression of SV fused with eGFP (red). pAAV-CVM-eGFP (control) and pAAV-CMV-SVeGFP (vaccine protein) plasmid were used

Calculated DNA and RNA copy number

A standard curve was obtained using standard dilutions (y-axis) and Ct values (x-axis), with the equation $y = -0.3271x + 14.548$ ($R^2 = 0.9975$). Copy number/mL of control and subunit vaccine viruses were 1.19×10^{11} and 1.05×10^{11}, respectively. For RNA copy number, another standard curve was $y = -0.262x + 10.341$ ($R^2 = 0.9963$), with RNA copy numbers of 5.96×10^{9} (control) and 1.18×10^{11} (subunit vaccine). An intramuscular dose of 200 µL in mice was suggested, which had 1.19×10^{9} (control) and 2.36×10^{10} (subunit vaccine) copies (Fig. 11).

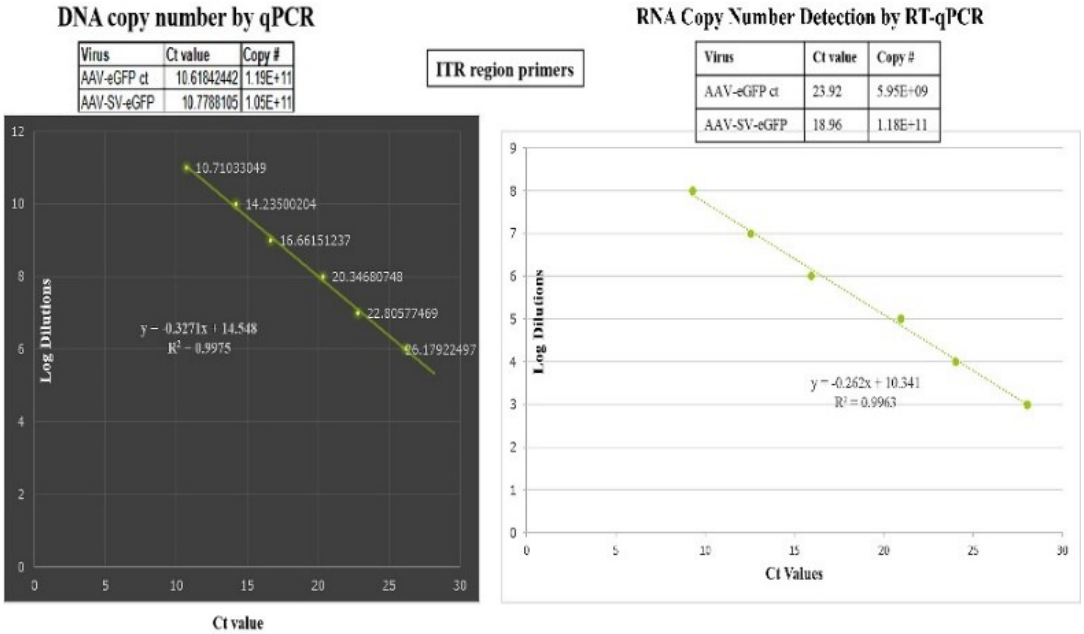

Fig. 11: DNA (left) and RNA (right) copy number detections

Titer limits of the two viruses were established through 10-fold serial dilution in 96-well plates to determine the lowest level of dilution that eGFP expression is still detectable. In this research, eGFP expression was detectable up to the 10^3 dilution level (Fig. 12). For comprehensive vaccine analysis, functional characterization of its proteins is also important, especially interactions with the host genome, regulation of immunity, and survivability of Mtb.

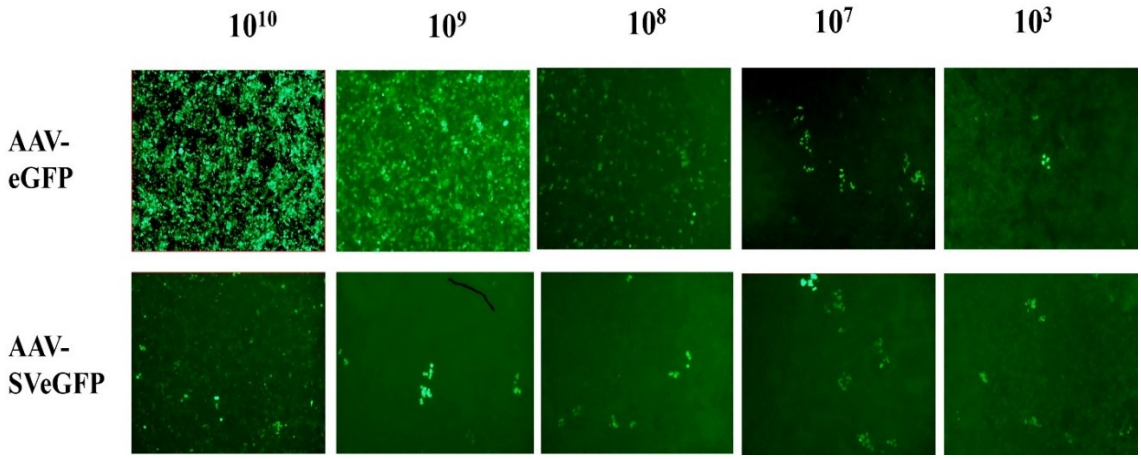

Fig. 12: AAV-eGFP and AAV-SV-eGFP viruses' 10-fold serial dilution

Discussion

Vaccination is a cost-effective way of preventing disease (38). An effort is made to develop a subunit vaccine against Mtb by incorporating three secretory systems' epitopes: TAT, Sec, and Esx. Unlike whole-organism vaccines, in this approach, highly immunogenic epitopes are used alone. The immunoinformatics-designed vaccine was validated using in silico analysis for in vitro and in vivo studies (8). Mtb pathogenesis is mainly controlled by secretory proteins that influence host immune processes (39). Epitopes were selected according to MHC-I/II binding and B-cell recognition. MHC-I is similar to CD8+ T cells, whereas MHC-II presents proteins to CD4+ T cells (40, 41).

Immunoinformatics analysis was confirmed with good vaccine binding to MHC-I, MHC-II, and B-cell epitopes. Homology modeling and Ramachandran plot analysis proved a stable 3D structure. TLR2 docking confirmed good binding affinity and stability. Efficient transcription and translation were accomplished using codon optimization (42). The ultimate construct contained 18 epitopes on a 576-amino acid sequence that has outstanding stability, high immunogenicity, and TLR2 binding. Reverse translation of the protein sequence and subcloning into an AAV Dj/8 helper-free bicistronic vector were carried out for expression in eukaryotic hosts. This 4.7 kb single-stranded DNA construct contains two terminal repeats (ITR), and successful cloning of the gene was established by qPCR (43, 44). High protein expression, copy number, and viral titer were proven by in vitro experiments. So are thus a possible candidate to be added to BCG for in vivo trials.

The COVID-19 pandemic severely affected TB diagnosis and treatment worldwide. Reduced access to health and resource redistribution caused a 15-20% reduction in TB case notifications in Iran during 2020, increasing community transmission and DR-TB incidence (45, 46). TB diagnosis went down by 30% due to prioritization of COVID-19 PCR tests (47). Limitations on movements and health overload delayed drug provision, raising the risk of MDR-TB (49). Iran's

completion rate was reduced by 10%, and DOTS program disruption increased nonadherence to 15% from 5-7% (46). TB death rose by 5-8%, with TB-COVID-19 patients having 20-25% higher mortality (50). Amplified surveillance, amplified diagnostics, and digital health solutions are the way forward to overcome these reversals (45, 48).

Conclusion

This study describes a comprehensive approach to the development of a novel subunit vaccine, characterized by a composite of highly immunogenic and non-allergic peptide epitopes that underwent in-depth in silico analysis, confirming its stability and strong binding affinity with the host cell surface receptor TLR2. The AAV virus and terminal repeat regions (ITR) exhibited optimal expression in host cells during in vitro analysis, displaying promising titers and copy numbers. The success of gene cloning was confirmed using qPCR, setting the stage for in vivo trials.

Journalism Ethics considerations

Ethical issues (Including plagiarism, informed consent, misconduct, data fabrication and/or falsification, double publication and/or submission, redundancy, etc.) have been completely observed by the authors.

Acknowledgements

We highly acknowledge the National Key Research and Development Program of China, the National Natural Science Foundation of China, and the Huazhong Agricultural University Scientific and Technological Self-innovation Foundation.

Conflict of Interest

The authors declare that there is no conflict of interests.

References

1. World Health Organization (2019). Global Tuberculosis Report 2019. Geneva, Switzerland. World Health Organization.
2. Behera D (2010). *Textbook of pulmonary medicine*. 2nd ed. New Delhi: Jaypee Brothers Medical Publishers.
3. Stephanie F, Saragih M, Tambunan USF (2021). Recent progress and challenges for drug-resistant tuberculosis treatment. *Pharmaceutics*, 13(5): 592.
4. Sethi G, Varghese RP, Lakra AK, et al (2024). Immunoinformatics and structural aided approach to develop multi-epitope based subunit vaccine against Mycobacterium tuberculosis. *Sci Rep*, 14(1): 15923.
5. Awasthi A, Sharma G, Agrawal P (2022). *Computational approaches for vaccine designing. In: Bioinformatics*. Academic Press, pp. 317-335.
6. Crampin AC, Glynn JR, Fine PE (2009). What has Karonga taught us? Tuberculosis studied over three decades. *Int J Tuberc Lung Dis*, 13(2):153–64.
7. Glick BR, Delovitch TL, Patten CL (2014). *Medical Biotechnology*. Washington DC: ASM Press, pp. 632-663.
8. Naeem MA, Adeel MM, Kanwal A, et al (2021) Reconnoitering Mycobacterium tuberculosis lipoproteins to design subunit vaccine by immunoinformatics approach. *Adv Life Sci*, 8(3): 300-306.
9. Pal R, Bisht MK, Mukhopadhya S (2022). Secretory proteins of Mycobacterium tuberculosis and their roles in modulation of host immune responses: focus on therapeutic targets. *FEBS J*, 289(14): 4146-4171.
10. da Costa C, Benn CS, Nyirenda T, et al (2024). Perspectives on development and advancement of new tuberculosis vaccines. *Int J Infect Dis*, 141S: 106987.
11. Braunstein M, Bensing BA, Sullam PM (2019). The two distinct types of SecA2-dependent export systems. *Microbiol Spectr*,

7(3): 10.1128/microbiolspec.psib-0025-2018.
12. Renshaw PS, Lightbody KL, Veverka V, et al (2005). Structure and function of the complex formed by the tuberculosis virulence factors CFP-10 and ESAT-6. *EMBO J*, 24(14): 2491-8.
13. Jackson M, Stevens CM, Zhang L, et al (2020). Transporters involved in the biogenesis and functionalization of the mycobacterial cell envelope. *Chem Rev*, 121(9): 5124-5157.
14. Zhu B, Dockrell HM, Ottenhoff THM, et al (2018). Tuberculosis vaccines: Opportunities and challenges. *Respirology*, 23(4): 359-368.
15. Lenz LL, Mohammadi S, Geissler A, et al (2003). SecA2-dependent secretion of autolytic enzymes promotes Listeria monocytogenes pathogenesis. *Proc Natl Acad Sci USA*, 100(21): 12432-7.
16. Saint-Joanis B, Demangel C, Jackson M, et al (2006). Inactivation of Rv2525c increases β-lactam susceptibility and virulence in Mycobacterium tuberculosis via the twin arginine translocation (Tat) system substrate pathway. *J Bacteriol*, 188(18): 6669-6679.
17. DiGiuseppe Champion PA, Cox JS (2007). Protein secretion systems in Mycobacteria. *Cell Microbiol,* 9(6): 1376-84.
18. Singh H, Ansari HR, Raghava GP (2013). Improved method for linear B-cell epitope prediction using antigen's primary sequence. *PLoS One*, 8(5): e62216.
19. Rahlwes KC, Dias BRS, Campos PC, et al (2023). Pathogenicity and virulence of Mycobacterium tuberculosis. *Virulence*, 14(1): 2150449.
20. Khalid K, Hussain T, Jamil Z, et al (2022). Vaccinomics-Aided Development of a Next-Generation Chimeric Vaccine against an Emerging Threat: *Mycoplasma genitalium*. *Vaccines*, 10(10): 1720.
21. Fadilah F, Paramita RI, Erlina L, et al (2022). *Linker optimization in breast cancer multiepitope peptide vaccine design based on molecular study*. In: 4th International Conference on Life Sciences and Biotechnology (ICOLIB 2021), Atlantis Press, pp. 528-538.
22. Arai R, Ueda H, Kitayama A, et al (2001). Design of the linkers which effectively separate domains of a bifunctional fusion protein. *Protein Eng*, 14(8): 529-32.
23. Livingston B, Crimi C, Newman M, et al (2002). A Rational Strategy to Design Multiepitope Immunogens Based on Multiple Th Lymphocyte Epitopes. *J Immunol*, 168(11): 5499-506.
24. Lennon-Duménil A-M, Bakker AH, Wolf-Bryant P, et al (2002). A closer look at proteolysis and MHC-class-II-restricted antigen presentation. *Curr Opin Immunol*, 14(1): 15-21.
25. Obaidullah AJ, Alanazi MM, Alsaif NA, et al (2021). Immunoinformatics-guided design of a multi-epitope vaccine based on the structural proteins of severe acute respiratory syndrome coronavirus 2. *RSC Adv*, 11(29): 18103-18121.
26. Byun EH, Kim WS, Kim JS, et al (2012). Mycobacterium tuberculosis Rv0577, a novel TLR2 agonist induces maturation of dendritic cells and drives Th1 immune response. *FASEB J*, 26(6): 2695-2711.
27. Hasan M, Azim KF, Begum A, et al (2019). Vaccinomics strategy for developing a unique multi-epitope monovalent vaccine against Marburg marburgvirus. *Infect Genet Evol*, 70: 140-157.
28. Wu CY, Monie A, Pang X, et al (2010). Improving therapeutic HPV peptide-based vaccine potency by enhancing CD4+T help and dendritic cell activation. *J Biomed Sci*, 17(1): 88.
29. Gasteiger E, Hoogland C, Gattiker A, et al (2005). *Protein identification and analysis tools on the ExPASy server*. In: The proteomics protocols handbook. Humana Press, pp. 571-607.
30. Saha S, Raghava GPS (2006). AlgPred: prediction of allergenic proteins and mapping of IgE epitopes. *Nucleic Acids Res*, 34 (suppl_2): W202-9.
31. Drage MG, Pecora ND, Hise AG, et al (2009). TLR2 and its co-receptors determine responses of macrophages and dendritic cells to lipoproteins of Mycobacterium tuberculosis. *Cell Immunol*, 258(1): 29-37.
32. Schneidman-Duhovny D, Inbar Y, Nussinov R, et al (2005). PatchDock and SymmDock: servers for rigid and symmetric docking. *Nucleic Acids Res*, 33 (suppl_2): W363-7.
33. Grote A, Hiller K, Scheer M, et al (2005). JCat: a novel tool to adapt codon usage of a target

gene to its potential expression host. *Nucleic Acids Res*, 33:W526-531.
34. Faust SM, Bell P, Cutler BJ, et al (2013). CpG-depleted adeno-associated virus vectors evade immune detection. *J Clin Invest*, 123(7): 2994-3001.
35. Rabinowitz J, Chan YK, Samulski RJ (2019). Adeno-associated virus (AAV) versus immune response. *Viruses*, 11(2): 102.
36. Zhu J, Huang X, Yang Y (2009). The TLR9-MyD88 pathway is critical for adaptive immune responses to adeno-associated virus gene therapy vectors in mice. *J Clin Invest*, 119(8): 2388-98.
37. Wiederstein M, Sippl MJ (2007). ProSA-web: interactive web service for the recognition of errors in three-dimensional structures of proteins. *Nucleic Acids Res*, 35 (suppl_2): W407-10.
38. Khatoon N, Pandey RK, Prajapati VK (2017). Exploring Leishmania secretory proteins to design B and T cell multi-epitope subunit vaccine using immunoinformatics approach. *Sci Rep*, 7(1): 8285.
39. Majlessi L, Prados-Rosales R, Casadevall A, et al (2015). Release of mycobacterial antigens. *Immunol Rev*, 264(1): 25-45.
40. Rothbard JB, Taylor WR (1988). A sequence pattern common to T cell epitopes. *EMBO* J, 7(1): 93-100.
41. Hewitt EW (2003). The MHC class I antigen presentation pathway: strategies for viral immune evasion. *Immunology*, 110(2): 163-9.
42. Makrides SC (1996). Strategies for achieving high-level expression of genes in Escherichia coli. *Microbiol Rev*, 60(3): 512-38.
43. Brument N, Morenweiser R, Blouin V, et al (2002). A versatile and scalable two-step ion-exchange chromatography process for the purification of recombinant adeno-associated virus serotypes-2 and -5. *Mol Ther,* 6(5): 678-86.
44. Grimm D, Lee JS, Wang L, et al (2008). In vitro and in vivo gene therapy vector evolution via multispecies interbreeding and retargeting of adeno-associated viruses. *J Virol*, 82(12): 5887-911.
45. World Health Organization (2022). WHO Global Task Force on TB Impact Measurement: report of a subgroup meeting on methods used by WHO to estimate TB disease burden, 11-12 May 2022, Geneva, Switzerland. World Health Organization.
46. Fallahi MJ, Nazemi M, Zeighami A, et al (2024). Changes in incidence and clinical features of tuberculosis with regard to the COVID-19 outbreak in Southern Iran. *BMC Infect Dis,* 24(1): 1043.
47. Sharafi M, TalebiMoghaddam M, Narouee S, et al (2024). Estimating the impact of the first 2 years of the COVID-19 pandemic on tuberculosis diagnosis and treatment outcomes in Southeastern City in Iran: an interrupted time series analysis of the preceding 10 years of ecological data. *BMC Health Services Research*, 24(1): 1489.
48. Sharifi Y, Ebrahimpur M, Payab M, et al (2022). The Syndemic Theory, the COVID-19 Pandemic, and The Epidemics of Non-Communicable Diseases (NCDs). *Medical Journal of the Islamic Republic of Iran*, 36:177.
49. Shahnavazi M, Rigi F, Heydarikhayat N (2022). Treatment Adherence and Influencing Factors in Patients with Tuberculosis during the COVID-19 Pandemic: A Mixed Method Study. *Health Education and Health Promotion*, 10(4): 633-642.
50. Aghajani J, Farnia P, Farnia P, et al (2022). Effect of COVID-19 pandemic on incidence of mycobacterial diseases among suspected tuberculosis pulmonary patients in Tehran, Iran. *Int J Mycobacteriol*, 11(4): 415-422.